Mo(VI) potential metallodrugs. Explaining the transport and cytotoxicity by chemical transformations

Monalisa Mohanty,[a] Atanu Banerjee,[a] Sudhir Lima,[a] Sushree Aradhana Patra,[a] Aurélien Crochet,[b] Giuseppe Sciortino,[c,d] Daniele Sanna,[e] Valeria Ugone,[e] Eugenio Garribba,*[c] and Rupam Dinda*[a]

[a] M. Mohanty, A. Banerjee, S. Lima, S. A. Patra, Prof. R. Dinda
Department of Chemistry,
National Institute of Technology, Rourkela,
769008 Odisha, India
E-mail: rupamdinda@nitrkl.ac.in
[b] Prof. A. Crochet
Department of Chemistry,
Fribourg Center for Nanomaterials,
University of Fribourg, CH-1700 Fribourg, Switzerland
[c] Dr. G. Sciortino, Prof. E. Garribba
Dipartimento di Chimica e Farmacia
Università di Sassari
Via Vienna 2, I-07100 Sassari, Italy
E-mail: garribba@uniss.it
[d] Dr. G. Sciortino
Institute of Chemical Research of Catalonia (ICIQ),
Avgda. Països Catalans, 16, 43007 Tarragona, Spain
[e] Dr. D. Sanna, Dr. V. Ugone
Istituto di Chimica Biomolecolare
Consiglio Nazionale delle Ricerche
Trav. La Crucca 3, I-07100 Sassari, Italy

Supporting information and the ORCID identification number(s) for the author(s) of this article can be found under: https://doi.org/10.1002/chem.xxxx.

Abstract: The transport and cytotoxicity of molybdenum-based drugs have been explained with the concept of chemical transformation; a very important idea in inorganic medicinal chemistry but often not completely considered. Two monomeric $[MoO_2(L^1)(MeOH)]$ (**1**) $[MoO_2(L^2)(EtOH)]$ (**2**) and two mixed-ligand dimeric $[\{MoO_2(L^{1-2})\}_2(\mu\text{-}4,4'\text{-bipy})]$ (**3**-**4**) $Mo^{VI}O_2$ complexes were synthesized and characterized. The structures of the solid complexes were solved through SC-XRD, while their transformation in water was clarified by UV-Vis, ESI-MS and DFT. In aqueous solution **1**-**4** lead to the penta-coordinated $[MoO_2(L^{1-2})]$ active species after the release of the solvent molecule (**1**-**2**) or removal of the co-ligand 4,4'-bipy bridge (**3**-**4**). $[MoO_2(L^{1-2})]$ are stable in solution and do not react with serum bioligand nor with cellular reductants. The binding affinity of **1**-**4** towards DNA and HSA and their *in vitro* cytotoxicity were evaluated through analytical and computational methods. Interestingly, the μ-4,4'-bipy bridged complexes **3**-**4** were found to be more active than the monomeric **1**-**2**, due to their dissociation into two equivalents of $[MoO_2(L^{1-2})]$ and the cytotoxic 4,4'-bipy molecule. Interestingly, the μ-4,4'-bipy bridged complexes **3**-**4** were found to be more active than the monomeric **1**-**2**, due to the mixture of species generated that is $[MoO_2(L^{1-2})]$ and the cytotoxic 4,4'-bipy, after their dissociation.

Introduction

Despite the rapid development of anticancer drugs, cancer remains one of the leading causes of death worldwide. This is due to the associated disadvantages of prevalent chemotherapeutic drugs like high toxicity to normal cells, limited ranges of activities, acquired tumour resistance, and metastasis (secondary) cancers.[1] Therefore, in an attempt to replace these drugs with suitable alternatives, numerous transition metal complexes are being synthesized and tested for their anticancer activities.

For the design and evaluation of the action mechanism of new metallodrugs, transport in the bloodstream and the binding to cellular targets are the key steps. In blood, serum albumins are the most abundant soluble proteins in higher animals and play many crucial physiological functions. These proteins tend to increase the solubility of hydrophobic compounds in plasma and regulate their delivery to target cells. Consequently, properties like absorption, stability, distribution, metabolism and toxicity of the pharmacological active metallocompounds can be significantly affected by their binding to serum albumins.[2] On the other hand, DNA is the primary target of many metal based anticancer drugs.[3] Metal complexes may bind to DNA leading to alteration and/or inhibition of DNA functioning.[4]

Although considerable attention is paid toward the interaction of metal complexes with biomolecules and their transport processes to the target tissues, their possible transformation in aqueous solution is often not completely taken into account during the design stage and when new potential metallic anticancer agents are tested. While for organic drugs the chemical changes are overlooked and it is often assumed that the administered compound reaches the target organs in an unaltered form, the situation is different for metal-based drugs, for which ligand exchange, hydrolysis, chemical bond breaking and redox reactions can occur in the biological media. Therefore, these processes must be taken into account to explain the experimental results. The importance of these transformations can be demonstrated for cisplatin *cis*-$[Pt(NH_3)_2Cl_2]$ and oxaliplatin [Pt(dach)(oxalato)], which, upon hydrolysis, lose the labile chloro and oxalato ligands, respectively, to form the active moiety *cis*-$Pt(NH_3)_2^{2+}$ and

$Pt(dach)^{2+}$ that interact with DNA.[5] A similar situation was also observed with titanocene, Cp_2TiCl_2.[6] Other studies on Pt-, Au-, Ru- and Rh-based potential drugs pointed in the same direction, identifying the active moieties involved in the ligand exchange or protein-metalation.[7] On the other hand, other facts must also be taken into account: polynuclear Au(III), Pd(II), Pt(II) complexes have higher cytotoxicity than mononuclear species,[8] and many dimeric and polymeric copper compounds have been described as very promising candidates,[9] without considering their dissociation in mononuclear units that was demonstrated unambiguously in aqueous solution and coordinating solvents by EPR spectrosopy.[10]

Recently, our groups have established that the enhanced protein interaction and cytotoxicity measured for few oxido and non-oxido vanadium complexes are due to the presence of several species in cell media and not (only) for the intact complexes.[11] Though the importance of the chemical transformations has been studied for several metals like vanadium (for instance, the anti-diabetic non-oxido V^{IV} complexes are active only if they transform into the $V^{IV}O$ form which is able to inhibit the protein tyrosine phosphatases[12]), little attention has been paid to the understanding of these factors for molybdenum(VI) complexes.[13]

Potential molybdenum based anticancer agents have been synthesized in oxidation states of +II, +V and +VI over the last few years.[14] They could reach the nucleus in an intact form and interact with DNA. Recent studies on the anticancerogenic activity of Mo^{VI} complexes have demonstrated that they have a binding affinity toward CT DNA, showing a good cytotoxic action on the cell lines HT-29 (human colon cancer) and HeLa (human cervical cancer).[15] Alternatively, the activity of these species can be related to their capability to produce reactive oxygen species (ROS) in solution, which cause cell damages to DNA, lipid peroxidation and cellular signal alteration.[16] Mo^{VI} compounds could be reduced in the cellular environment and give Mo^{V} species that is able to form ROS through a Fenton-like reaction $Mo^{V}O^{3+} + H_2O_2 \rightarrow Mo^{VI}O_2^{2+} + H^+ + {}^{\bullet}OH$; these results indicate that Mo^{V} could be the active species. Therefore, further experimental investigations on the precise mechanism of the potential molybdenum drugs in solution are needed to exploit their biological activity.

In continuation of our research on the pharmacological properties of various transition metal–hydrazone species,[11,15,17] herein, the synthesis of two monomeric $[MoO_2(L^1)(MeOH)]$ (**1**) $[MoO_2(L^2)(EtOH)]$ (**2**) and two mixed-ligand dimeric $[\{MoO_2(L^{1-2})\}_2(\mu\text{-}4,4'\text{-bipy})]$ (**3** and **4**) dioxidomolybdenum(VI) complexes from two aroylhydrazone ligands (H_2L^{1-2}) are reported. Hydrazones are important set of ligands, as they manifests a vast range of pharmaceutical activities.[18] It has been demonstrated that their biological properties are considerably enhanced upon complexation to metal ions.[19] Moreover, the introduction of nitrogen-chelating bidentate co-ligands with powerful σ donor functions, such as 4,4'-bipyridine might affect the planarity, hydrophobicity, and general anticancer action of metal complexes.[20] The interaction of the synthesized compounds with human serum albumin (HSA) and Calf Thymus DNA (CT DNA) has been studied. Further, studies on their antioxidant capability, redox properties, and molecular modeling calculations were also carried out. Finally, the Mo complexes were screened for their anticancer activity against human cervical cancer (HeLa) and human colon cancer (HT-29) and noncancerous mouse embryonic fibroblast (NIH-3T3) cell lines. Notably, the results can be related to the transformation of **1**–**4** in biological media and allow to discuss the importance of the chemical changes in the explanation of the pharmacological activity of metal-based potential drugs. To the best of our knowledge this is one of the first reports where such a comprehensive idea is applied to the pharmacological action of molybdenum complexes.

Results and Discussion

Synthesis

The synthetic procedure of **1**–**4** from two aroylhydrazone ligands containing a diethylamine substituent is represented in **Scheme 1**. Upon reaction of H_2L^{1-2} with $MoO_2(acac)_2$ in alcoholic medium, deep red crystals of **1** and **2** were obtained from slow evaporation of the filtrate, while the addition of 4,4'-bipyridine as a co-ligand in acetonitrile medium to the above reaction mixture yielded reddish brown crystals of **3** and **4** directly from the reflux conditions.

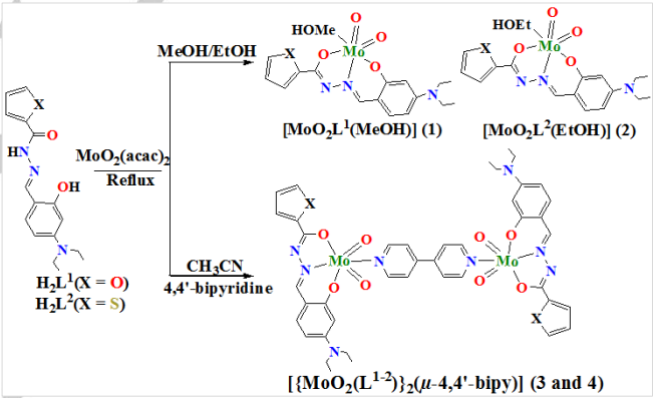

Scheme 1 Schematic representation for the synthesis of $[MoO_2(L^1)(MeOH)]$ (**1**), $[MoO_2(L^2)(EtOH)]$ (**2**), and $[\{MoO_2(L^{1-2})\}_2(\mu\text{-}4,4'\text{-bipy})]$ (**3** and **4**).

X-ray structure description

In order to predict a specific coordination mode of H_2L^{1-2} or stereochemistry for the monomeric Mo^{VI} complexes, the structures of **1**–**4** were determined through X-ray crystallography. The crystal data and structure refinement details are given in **Table S1**. The solid state structures of the complexes **1** and **2** are shown in **Figure 1** and **S1** and the selected bond lengths and bond angles are enlisted in **Table S2** and **S3**.

The crystal lattice of complex **1** is composed of two units with identical coordination geometry, differing only in the position of the alkyl chains. The structures of **1** and **2** (**Figure 1** and **S1**) reveal that the ligand is coordinated to $Mo^{VI}O_2^{2+}$ ion as an O,N,O-donor, with bite angles of ~71° and ~82° for O(1)–Mo(1)–N(2) and O(2)–Mo(1)–N(2), respectively (**Table S2** and **S3**). Further, a solvent molecule is also coordinated to the metal center in *trans* to one Mo=O bond; therefore, the complex can be formulated as $[MoO_2(L^1)(MeOH)]$ (**1**) $[MoO_2(L^2)(EtOH)]$ (**2**) where L refers

to an aroylhydrazone ligand. This composition is found to be consistent with the microanalytical data. In these structures, the coordination geometry around molybdenum center can be described as distorted octahedral as given in the bond parameters around the metal center. Solvent molecule like methanol and ethanol completes the distorted octahedral coordination sphere of **1** and **2** and provides stability to the system in solid state. The Mo=O, Mo–O, Mo–N, C=N and N–N bond lengths are within the normal range for Mo^{VI}–L fragment.[21] The longer bond length of Mo–O(Solv) found in these complexes in comparison to the normal single bond length [2.354(3) Å against 1.932(3)–2.024(3) Å], indicates a weak site available for substitutions (**Table S2** and **S3**). This feasibility is realized in the facile formation of adducts with formula [{$MoO_2(L^{1-2})$}$_2$(μ-4,4'-bipy)] (**3** and **4**).

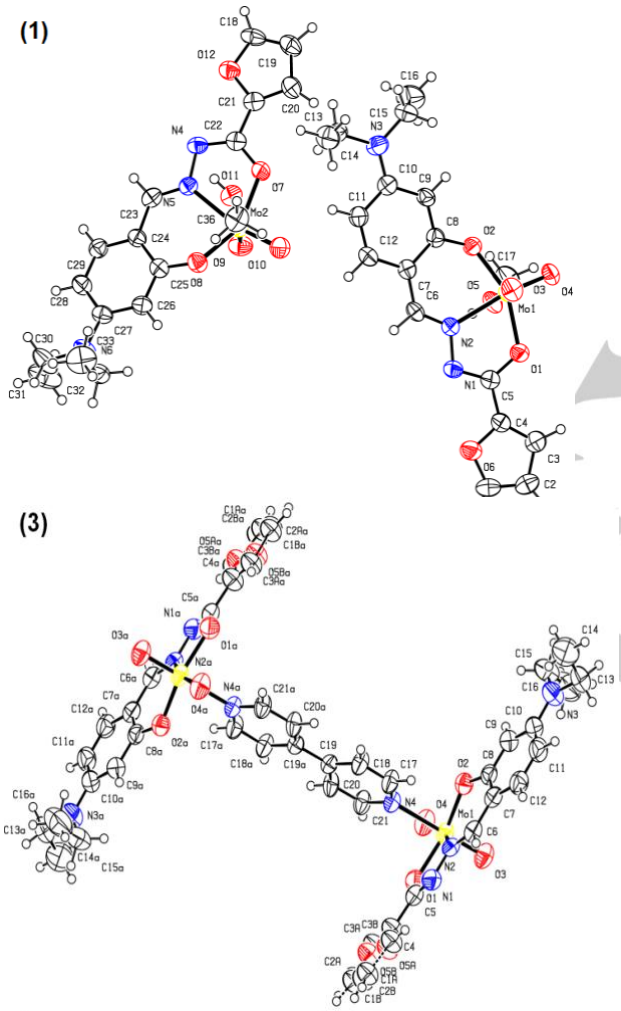

Figure 1 Molecular structures of the complex **1** and **3** with atomic numbering scheme used.

On the other hand, the dimeric complexes [{$MoO_2(L^{1-2})$}$_2$(μ-4,4'-bipy)] (**3** and **4, Figure 1** and **S1**) crystallize in orthorhombic crystal system and Pbca space group, while the molecule is present in a crystallographic center of inversion. Each half of the dimeric structure is identical to the other one. There is a distorted octahedral coordination environment around the Mo^{VI} center, where the dianionic and tridentate ligand $(L^{1-2})^{2-}$ with its meridionally situated donors O(1), N(2) and O(2) lay in the equatorial plane along with the oxido ligand O(3) for **3** and O(4) for **4**. The Mo–O distances range from 1.700(3)–1.698(4) Å for the oxido ligand O(4) for **3** and O(3) for **4**, located in an axial position, and 1.912(3)–1.921(3) Å for the phenolato oxygen O(2). The Mo(1)–O(1)(enolato) distance is 2.001(3)–2.007(4) Å, while the second axial position is held by a nitrogen atom of the bridging 4,4'-bipyridine ligand, and is observed to be significantly further from the Mo center than the other five ligated atoms. Mo(1)–N(4), at 2.420(3)–2.421(4) Å, is the most long of all the six Mo–L bonds and, therefore, the most susceptible to ligand exchange.[21c] The chelate bite angles for the five- and six-membered rings have values within the expected ranges [O(2)–Mo(1)–N(2), 81.83(14)°; O(1)–Mo(1)–N(2), 71.57(14)°] (**Table S3**).

Spectral characteristics

Spectral characteristics of the ligands (H_2L^{1-2}) and complexes **1**–**4** have been listed in the *Experimental Section* reported in the Supporting Information. FT-IR spectra of the complex exhibit two stretching bands in the range 917–941 cm^{-1} indicating the dioxido nature of MoO_2^{2+} ion.[17d,21b,22] Electronic spectra of the complexes display strong or moderate intensity bands in the range 475–478 nm and 354–360 nm due to ligand to metal charge transfer (LMCT) and ligand centered transitions, respectively.[17d,21b,22] The representative absorbance spectrum of **2** is given in **Figure S2**. In comparison to the signals of the ligands, NMR spectra of the complexes show a disappearance of –OH and –NH protons due to deprotonation and coordination of the metal atom. Monomeric complexes **1** and **2** exhibited additional peaks in the expected region for the axially coordinated MeOH and EtOH molecule. Besides, there is an increased number of resonances in the aromatic region for the dimeric complex **3** and **4** as compared to its free ligands H_2L^{1-2} which is due to the coordinated co-ligand 4,4'-bipy. Due to their center of symmetry, resonance peaks of only one half of the molecule are visible in the spectra.

The ^{13}C NMR signals of the complexes, as depicted in the *Experimental section* of the Supporting Information, confirm that the coordinated labile solvent molecule (alcohol) for **1** and **2** remains coordinated in an organic solvent like DMSO. In the downfield region (δ = 156.07-99.56 ppm) an increased number of aromatic carbon peaks for complexes **3** and **4**, in comparison to their corresponding ligand backbone, is also evident of the presence of the 4,4'-bipy co-ligand in the vicinity of the metal and also supports that the two structurally characterized dimeric complexes retain their identity in DMSO.

Stability in aqueous solution: spectroscopic/spectrometric behavior and DFT calculations

The stability of all the complexes has been established in water through UV-Vis spectroscopy, ESI mass spectrometry and DFT methods. The electronic absorption spectra recorded as a function of the time on **1**–**4** in 50 mM Tris-HCl buffer at pH 7.4 are depicted in **Figure S3**. The first thing that must be noticed is that they are different compared to those in DMSO. This suggests that the complexes **1** and **2** probably lose the weak axial solvent

molecule. The transformation is almost instantaneous and, once it happens, there are no further changes observed over time. The behavior of **3** and **4** is similar (**Figure S3**): each series of spectra is different with respect to that recorded in DMSO solution and do not change after 48 h.

Overall, the results can be rationalized postulating that these complexes are not stable in aqueous solution and probably **1** and **2** lose the weak axial solvent molecule, while for **3** and **4** the breaking of the μ-4,4'-bipy bridge occurs. The comparison of the spectra indicates that **1** and **3** on one hand (λ_{max} = 380-381 nm) and **2** and **4** on the other (λ_{max} = 383−384 nm) behave similarly; therefore, from these data, it can be argued that **1** and **3** form the mononuclear species $[Mo^{VI}O_2(L^1)]$ and **2** and **4** $[Mo^{VI}O_2(L^2)]$.

ESI-MS spectra of the complexes **1**–**4** were recorded in a mixture MeOH/H_2O 90/10 v/v in the positive-ion mode. It was not possible to record the spectra in water alone for the scarce solubility of the metal species. The characteristic pattern of molybdenum, due to ^{92,94,95,96,97,98,100}Mo isotopes, allows to assign unequivocally the nature of the signals (see **Figure 2** and Supporting Information **Figure S4-S6**).

For **1** and **2** the "molecular ion" peaks are observed at m/z 452.01 and 467.99 respectively and are attributed to the adducts $[MoO_2(L^{1-2})]+Na^+$ (**Table S4** and **Figure S4-S5**), suggesting that the solvent ligand (MeOH for **1** and EtOH for **2**), weakly bound in the axial position, is removed in water according to the reaction (1). No m/z signals assignable to $[MoO_2(L^{1-2})(Solv)]$ were observed. Less intense peaks of proton and potassium adducts, $[MoO_2(L^{1-2})]+H^+$ (at 430.03 and 446.01 m/z for **1** and **2** respectively) and $[MoO_2(L^{1-2})]+K^+$ (at 467.99 and 483.96 m/z for **1** and **2** respectively) were also identified. The comparison between the experimental and calculated isotopic pattern for $[MoO_2(L^{1-2})]+H^+/Na^+/K^+$ ion peaks is shown in **Figure S7** and **S8**.

$$[MoO_2(L^{1-2})(Solv)] \xrightarrow{water} [MoO_2(L^{1-2})] + Solv \quad (1)$$

The complexes **3** and **4** (in MeOH/H_2O 90/10 v/v) show signals similar to **1** and **2**, respectively (**Table S5** and **Figure 2** and **S6**). In particular, the peaks of $[MoO_2(L^{1-2})]+H^+/Na^+/K^+$ were revealed plus an intense absorption attributable to [4,4'-bipy]$+H^+$ at m/z = 157.08, suggesting that in solution **3** and **4** transform to $[MoO_2(L^{1-2})]$ and 4,4'-bipy (reaction (2)). No peaks attributable to $[\{MoO_2(L^{1-2})\}_2(\mu$-4,4'-bipy)] in the m/z range 1000-1100 were found and this indicates that in methanol/water the reaction (2) is completely shifted toward right.

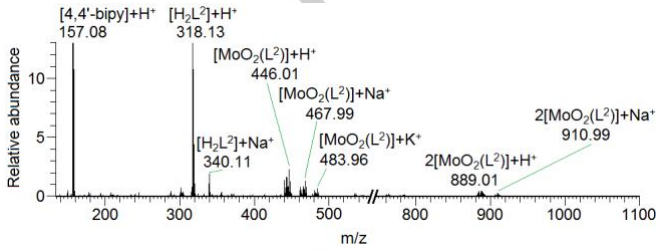

Figure 2 ESI-MS spectrum recorded in the positive ion mode dissolving the complex **4** in a mixture MeOH/H_2O 90/10 v/v, 50 μM.

$$[\{MoO_2(L^{1-2})\}_2(\mu\text{-}4,4'\text{-}bipy)] \xrightarrow{water} 2[MoO_2(L^{1-2})] + 4,4'\text{-}bipy \quad (2)$$

To confirm these insights, the speciation of **1**–**2** and **3**–**4** in aqueous media has been also studied by computational methods evaluating the relative stability of the species $[Mo^{VI}O_2(L^{1-2})(Solv)]$, $[\{Mo^{VI}O_2(L^{1-2})\}_2(\mu$-4,4'-bipy)] and $[Mo^{VI}O_2(L^{1-2})]$, where Solv is MeOH, EtOH and H_2O. The solvent effect was included in the framework of the SMD model.[23]

Notably, the results indicated that the reactions (1-2) are strongly shifted towards right in agreement with ESI-MS measurements. In the hexa-coordinated species $[MoO_2(L^{1-2})(MeOH/EtOH/H_2O)]$, the monodentate O-ligands leave spontaneously the axial site and cannot be characterized as energy minima. From this finding, it can be argued that ΔG_{aq} is very negative for reaction (1). For the sake of the completeness, the simulations were repeated for **1** in MeOH continuum model; the results indicated that it remains coordinated up to a distance Mo–O(MeOH) of 3.260 Å. For larger distances, methanol spontaneously leaves the axial site, suggesting that the weak MeOH coordination observed in the X-ray structure should be ascribed to solid state aggregation and stabilization effects in the crystal lattice. Similarly, the dissociation of $[\{MoO_2(L^{1-2})\}_2(\mu$-4,4'-bipy)] (reaction (2)) is highly favorable with ΔG_{aq} values of -26.4 and -25.7 kcal mol^{-1} for **3** and **4**, respectively. From this analysis, it can be inferred that in aqueous solution the two 5-coordinated species $[MoO_2(L^1)]$ (from **1** and **3**) and $[MoO_2(L^2)]$ (from **2** and **4**) are formed. The optimized structure of $[Mo^{VI}O_2(L^{1-2})]$ is shown in **Figure S9**; the electronic and Gibbs energies of the species involved in the equilibria are reported in **Table S6**, while the ΔG values in aqueous solution for the reactions (1) and (2) are shown in **Table S7**.

Binding to serum bioligands with low molecular mass

For a potential metallodrug, the study of the interaction with serum bioligands is essential to ascertain its possible biotransformation and transport of the active species in blood up to the target cells. Obviously, proteins play an important role, in particular HSA (see *infra*), but the involvement of low molecular mass bioligands (bL) cannot be ignored. Among the serum bL, citrate (citr), lactate (lact), and amino acids, especially histidine (His) may interact with $[MoO_2(L^{1-2})]$ to form ternary $Mo^{VI}O_2$–L^{1-2}–bL species or the corresponding binary complexes $Mo^{VI}O_2$–bL. The systems were explored by electronic absorption spectroscopy in mixtures H_2O/MeOH 90/10 v/v, 80/20 v/v and 50/50 v/v varying the pH (5.0 and 7.4), and metal concentration (50 and 10 μM). The results indicated that no binding occurs (**Figures S10-S11**) and $[MoO_2(L^{1-2})]$ do not form ternary species with the examined bioligands.

HSA binding

UV-Vis absorption study

After a potential metal-containing drugs is administered (orally or intravenously), it enters the bloodstream where the binding with blood carrier proteins such as HSA plays a significant role in assessing its potentiality as a drug. The

strength of these interactions can determine the overall pharmacokinetic properties of the drugs, such as storage, transport and removal, thereby regulating its efficiency.[24]

Fluorescence quenching study

Fluorescence spectroscopy is commonly used to study the binding of potential drugs with serum proteins and to get information on their structure and dynamics in the presence of metal complexes.

Fluorescence emission spectra of HSA, containing one tryptophan moiety, were recorded in the absence and presence of the Mo complexes (quenchers) in 50 mM Tris-HCl buffer (pH 7.4). The intrinsic fluorescence intensity of HSA was significantly quenched upon the gradual addition of increasing concentration of the quencher accompanied with hypsochromic shifts of 10, 14, 11 and 10 nm for the complexes **1**, **2**, **3** and **4**, respectively (**Figure 3** and **S12-S13**). In order to quantitatively estimate the magnitude of interaction between the compounds and HSA, the data were analyzed using the Stern-Volmer equation, which includes a bimolecular quenching rate constant and average life time of the fluorophore as shown in the following equation:[25]

$$\frac{F_0}{F} = 1 + k_q \tau_0 [Q] = 1 + K_{SV}[Q] \quad (3)$$

where F and F_0 are the fluorescence intensities with and without the quencher respectively, k_q the bimolecular quenching rate constant, τ_0 the average lifetime of fluorophore in the absence of a quencher and [Q] the concentration of a quencher, *i.e.* the Mo species. K_{SV} is the Stern–Volmer quenching constant in M^{-1}. The quenching constants K_{SV} for the complexes are collected in **Table 1**. Furthermore, the linear curve of F_0/F versus [Q] also suggests a static quenching, i.e. formation of fluorophore quencher adducts in the ground state. In protein binding studies, the binding constant (from the intercept) and number of binding sites (from the slope) were obtained using the Scatchard equation, given by:

$$\log \frac{F_0 - F}{F} = \log K_a + n \log[Q] \quad (4)$$

where K_a and n are the binding constant and number of binding sites, respectively. It has been demonstrated above, the monomeric and dimeric complexes form one and two equivalents of the penta-coordinated [$MoO_2(L^{1\text{-}2})$] species respectively along with the release of the solvent molecule (**1** and **2**) and the co-ligand 4,4'-bipy (**3** and **4**). Hence, for the calculation of the various binding parameters, one mole for monomeric and three moles for the dimeric complexes, considering the contributions to the fluorescence of [$MoO_2(L^{1-2})$] and 4,4'-bipy, were taken up (**Figure 3** and **S12-S13**). It is noticed that the values of binding constants for monomeric complexes **1** and **2** were close to each other, and similar observation were also made for dimeric complexes **3** and **4**. Though, as per our above rationale, the monomeric and dimeric complexes should have identical binding constants, but experimentally a variance was observed. Overall, the binding constants of the complexes show a reversible binding and release of the complex from HSA. The number of binding sites for all the complexes was found to be ~1.

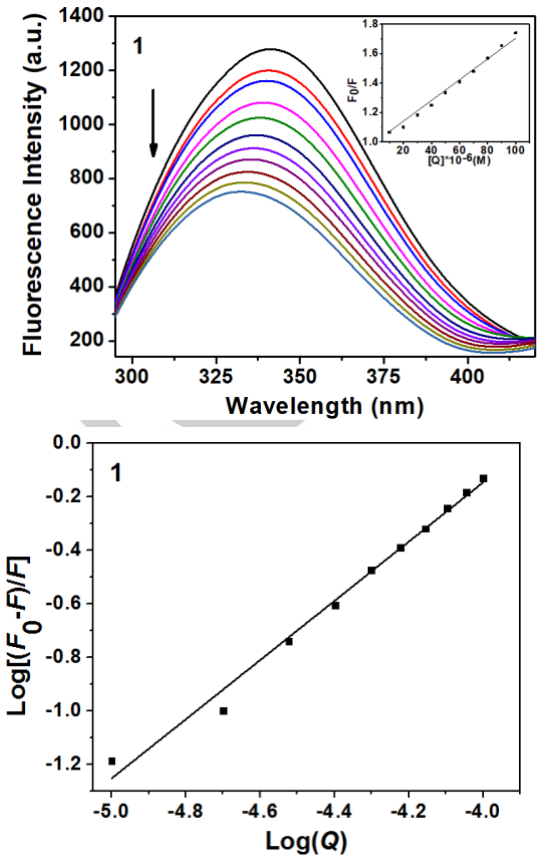

Figure 3 Fluorescence quenching of HSA (10 μM) along with successive addition of 10 μM for complex **1** (0–100 μM) with its Stern-Volmer plot in the inset. Arrow indicates the decrease in fluorescence intensity with respect to an increase in complex concentration. Scatchard plot of **1** is shown below.

Table 1 Parameters obtained from HSA interaction study for complexes **1**–**4**.

Parameter	Complex			
	1	**2**	**3**	**4**
K_{SV} (M^{-1})	(7.04 ± 0.13)×10^3	(6.80 ± 0.26)×10^3	(4.96 ± 0.10)×10^3	(3.66 ± 0.20)×10^3
k_q (M^{-1} s^{-1})	(1.13 ± 0.16)×10^{12}	(1.10 ± 0.26)×10^{12}	(8.02 ± 0.15)×10^{11}	(5.92 ± 0.21)×10^{11}
K_a (M^{-1})	(1.86 ± 0.17)×10^4	(1.37 ± 0.22)×10^4	(9.33 ± 0.19)×10^4	(2.75 ± 0.24)×10^4
n	1.10 ± 0.04	0.89 ± 0.03	1.35 ± 0.02	1.24 ± 0.01

K_a values, in the range 10^4, highlight a low or moderate interaction of the Mo species with HSA that may lead to a reduction in bioavailability taking into account only the free drug can diffuse across cell barriers and reach therapeutic targets.[26] Therefore, HSA may be considered as a good carrier for complexes **1**–**4**,[27] while a higher binding affinity would inhibit the subsequent release of the potential drug, leading to a decrease of *in vivo* anticancer activity.

DFT and docking calculations

The binding of Mo complexes **1**–**4** to HSA was also studied by DFT and docking calculations. We demonstrated above

that **1**–**3** and **2**–**4** undergo transformation in aqueous solution to give the penta-coordinated species $[Mo^{VI}O_2(L^1)]$ and $[Mo^{VI}O_2(L^2)]$, which – in the bloodstream – could react with HSA in two ways, through a *coordinative* or a *non-covalent binding* on the protein surface. To evaluate the possibility of formation of a *coordinative binding* through His or Asp/Glu residues, the reaction (5) was considered:

$$[Mo^{VI}O_2(L^{1-2})] + MeIm/AcO^- \rightleftarrows [Mo^{VI}O_2(L^{1-2})(MeIm/AcO)]^{x-} \quad (5)$$

where 1-methylimidazole (MeIm) and acetate (AcO^-) are models for the binding of His-N or Asp/Glu-COO to molybdenum and x = 0 for MeIm and x = 1 for AcO^-. The solvent effects were considered through the SMD model for water.[17] The values of ΔG_{aq} for the formation of $[Mo^{VI}O_2(L^{1-2})(MeIm)]$ and $[Mo^{VI}O_2(L^{1-2})(AcO)]^-$ are in the range 11.5-12.6 kcal mol^{-1}, inducing us to discard the possibility that 6-coordinated species are formed in solution (**Table S7**). These results suggest that the direct coordination of amino acid side-chain of a protein is disfavoured and that HSA interacts with Mo species only in a non-covalent mode. For this reason, only $[Mo^{VI}O_2(L^1)]$ was used as a model for the classical (non-covalent) blind docking assay.

Docking results for $[Mo^{VI}O_2(L^1)]$ with fatted HSA highlight several clusters with similar scoring values (F_{max} ranging from 16.2 to 20.0 GoldScore units), indicating the absence of binding specificity. This is in line with the intermediate-low values of the binding constants K_a (**Table 1**). The best solutions are located at the interfaces of subdomains IIIA/IB (**Figure 4a**) and IIA/IB (**Figure 4b**); others are found at interface IIIA/IIIB (**Figure 4c**). Each structure is stabilized by at least one hydrogen bond between the aza or O_{furan} functionalities of $(L^1)^{2-}$ and/or the oxido ligands with OH groups of Tyr or NH groups of Asn, Lys or Arg residues (**Table 2**). It must be highlighted that interfaces IIIA/IB and IIIA/IIIB define an internal pocket in HSA, reported as a common site for ligand interactions including metal species.[28] Interestingly, the adducts formed at these sites indicate that the molybdenum species are close to the unique tryptophan (Trp214) of the protein, in agreement with fluorescence quenching experimentally observed.

Table 2 Blind docking results for the interaction of $[Mo^{VI}O_2(L^1)]$ with fatted human serum albumin.

Region	F_{max}[a]	F_{mean}[b]	Interactions	Pop.[c]	Rank
IIIA/IIIB	20.00	19.12	NH_3^+,Lys541···NN; $NH_{2,Arg410}$···MoO_{ax}	4	I
IIA/IB	19.44	17.11	$NH_{2,Arg222}$···NN; NH_3^+,Lys195···MoO_{ax}	97	II
IIIA/IB	19.30	18.11	NH_2,Arg196···$MoO_{ax/eq}$; $NH_{2,Gln459}$···MoO_{eq}	13	III
IIIA/IIIB	17.59	16.62	NH_3^+,Lys541···MoO_{ax}; $NH_{2,Arg410}$···MoO_{eq}	21	V
IIIA/IIIB	17.28	16.26	NH_3^+,Lys541···MoO_{eq}; NH,Arg410···MoO_{ax}	60	IV
IIIA/IB	16.88	16.14	NH_3^+,Lys195···NN/O_{furan}; OH_{Tyr452}···MoO_{eq}	85	VI
IIA/IB	16.21	15.45	NH_2,Arg257···MoO_{ax}	18	VII

[a] *Fitness* value for the most stable pose of each cluster (F_{max}). [b] Mean *Fitness* value of the GoldScore scoring function for each cluster (F_{mean}). [c] Number of solutions in the identified cluster.

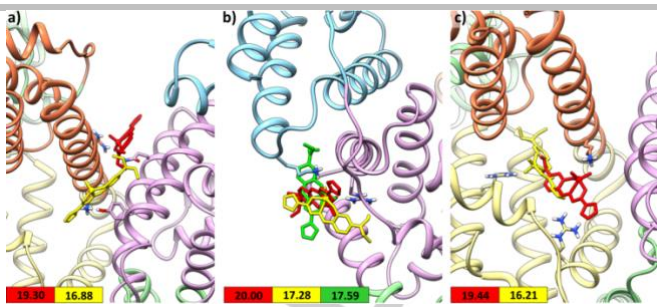

Figure 4 Best representative solutions of the most stable clusters for the interaction of $[Mo^{VI}O_2(L^1)]$ with fatted HSA: a) subdomains IIIA/IB; b) subdomains IIIA/IIIB; c) subdomains IIA/IB, interfaces. Subdomains IIA, IIIA, IB and IIIB, are depicted in yellow, purple, brown and cyan, respectively. Interacting residues are shown and F_{max} values are reported for each cluster with corresponding colors.

Förster resonance energy transfer (FRET)

In the above section, we mentioned that the molybdenum species are close to the unique tryptophan (Trp214) of HSA. Therefore, fluorescence resonance energy transfer (FRET) was used to estimate the distance between the Trp214 residue and molybdenum species. FRET constitutes a non-destructive spectroscopic method that can provide useful information about the distance of a donor and an acceptor molecule.[29] According to Förster's nonradiative energy transfer theory, the efficiency of energy transfer between a donor and acceptor (*E*), and the average distance between them (r_0) can be calculated using eq. (6):[29a,30]

$$E = \frac{R_0^6}{R_0^6 + r_0^6} = 1 - \frac{F}{F_0} \quad (6)$$

where R_0 is the distance at 50% transfer efficiency, and F and F_0 are the observed fluorescence intensities of HSA in the presence and absence of Mo complexes, respectively (see Supporting Information for further details). The spectral overlap between the normalized donor emission spectrum of HSA and molar extinction coefficient spectrum of the acceptor complexes (**1**–**4**) is shown in **Figure S14** and the FRET parameters calculated from eq. (6) and (S1-S2) are summarized in **Table 3**.

Table 3 Förster energy transfer parameters for interactions of the complexes **1**–**4** with HSA.

Complex	*E*	*J* (nm^4 M^{-1} cm^{-1})	R_0 (nm)	r_0 (nm)
1	0.090	3.23×10^{14}	2.90	4.23
2	0.167	3.88×10^{14}	2.99	3.88
3	0.163	5.42×10^{14}	3.16	4.13
4	0.141	4.86×10^{14}	3.11	4.18

The values obtained for R_0 and r_0 are much less than 8 nm which is essential for FRET[31] to take place between donor (Trp214) and the specific molybdenum complex (acceptor) bound to HSA (as found from molecular docking study). Furthermore, the obtained r_0 value obeys the relation $0.5R_0 < r_0 < 1.5R_0$, which implies that the energy transfer takes place in the interaction with high probability.[31,32]

Antioxidant assays

DPPH assay

DPPH assay can be monitored using UV-Vis spectrophotometry and/or EPR spectrometry. The EC_{50} values for the ligands H_2L^1 and H_2L^2, obtained by spectrophotometric analysis are 378 and 96 μM, respectively; those obtained by EPR are 316 and 67 μM for the two ligands. The UV-Vis and EPR spectra obtained for H_2L^1 are reported in **Figures S15-S16.** Unfortunately, due to the low solubility of the complexes **1**–**4** in ethanol, the determination of their EC_{50} values is prevented. From a qualitative point of view, the results obtained for **1**–**4** with the two spectroscopic techniques are not exactly coincident; probably for the intense color of the complex solutions which interferes with the absorption at 517 nm.[33]

ABTS assay

The ABTS assay is based on the reactivity of antioxidants towards the radical cation $ABTS^{\bullet+}$ obtained by reacting 2,2'-azino-bis(3-ethylbenzothiazolin-6-sulfonic acid) with potassium peroxydisulfate. This radical has an absorption maximum, in ethanolic solution, at 734 nm, while its reduced counterpart does not absorb at this wavelength.[34] This assay is used to determine the TEAC (Trolox Equivalent Antioxidant Capacity) value of a specific antioxidant, which is a dimensionless value, particularly used because it allows comparing the antioxidant activity of different compounds, all referred to trolox. Trolox (6-hydroxy-2,5,7,8-tetra-methylchroman-2-carboxylic acid) is chosen because its structural similarity with vitamin E and good solubility in water. The TEAC values for the ligands H_2L^{1-2} and for the complexes **1**−**4** are reported in **Table 4**.

Since all the TEAC values are < 1, all the examined compounds (ligands and complexes) are less antioxidant than trolox. Notably, the ligands H_2L^{1-2} are more antioxidant than the respective complexes. The ligand H_2L^2 and the complexes containing it (**2** and **4**) are less antioxidant than H_2L^1 and the corresponding complexes (**1** and **3**); this effect is likely due to the replacement of the thiophene heterocycle by furan. The results obtained for H_2L^1 and H_2L^2 with the ABTS assay are not in agreement with those obtained with the DPPH assay. In the ABTS assay H_2L^1 results to be more antioxidant than H_2L^2, while in the DPPH assay the opposite is true.

This apparent anomaly is not surprising and can be related to the type of assay used for the determination of the antioxidant activity which reflects a particular reactivity towards a substrate in a specific solvent or mixture of solvents.[35]

Table 4 TEAC values of the ligands H_2L^{1-2} and of complexes **1**−**4**.

Compound	TEAC value
H_2L^1	0.977 ± 0.126
H_2L^2	0.805 ± 0.039
1	0.245 ± 0.002
2	0.067 ± 0.003
3	0.506 ± 0.011
4	0.274 ± 0.010

DNA binding

Absorption Titration

The cytotoxicity of metal complexes is often attributed to their ability to interact with DNA, changing its structure and stability by hydrogen bonding and π stacking between the strands.[36]

Electronic absorption spectroscopy is a conventional method used to investigate the interaction of metal complexes with DNA (covalent or non-covalent such as intercalation and electrostatic or groove binding).[37] On gradual addition of CT DNA to a solution containing 50 mM Tris–HCl buffer (pH 7.4) and the Mo complexes with constant concentration, an appreciable hypochromic shift is observed for the LMCT bands, while absorption bands in the region 275−390 nm show a hyperchromic effect along with a red shift of 8−15 nm (**Figure S17**). The hypochromicity observed in the spectra reveals the presence of charged cations which bind to DNA *via* an electrostatic attraction to the phosphate groups of the DNA backbone, thereby damaging its secondary structure. The hyperchromicity may be also assigned to external contact (electrostatic binding) or to partial uncoiling of the DNA double helical structure, exposing a higher number of its bases. Moreover, an isosbestic spectral change was also observed for **2**−**4**, which suggests the existence of a chemical equilibrium between the bound and unbound state of the complexes.[37a]

The hypochromic shifts in the LMCT absorption bands for each complex were chosen to determine their binding constant (K_b) using eq. (7):[38]

$$\frac{[DNA]}{\varepsilon_a - \varepsilon_f} = \frac{[DNA]}{\varepsilon_b - \varepsilon_f} + \frac{1}{K_b(\varepsilon_b - \varepsilon_f)} \quad (7)$$

where, ε_a, ε_f and ε_b are the apparent extinction coefficients of the complexes in the presence, in absence and to fully bound DNA, respectively, [DNA] is the concentration of DNA base pairs, and K_b is the intrinsic binding (equilibrium) constant. The values of K_b, calculated plotting [DNA]/(ε_a – ε_f) *vs.* [DNA], for the complexes **1**−**4** were $2.08 \pm 0.27 \times 10^4$, $1.40 \pm 0.39 \times 10^3$, $2.04 \pm 0.16 \times 10^4$ and $(2.11 \pm 0.40 \times 10^4)$ respectively. As described in the *Fluorescence quenching* section, here too, the contribution to the absorbance of two moles of $[MoO_2(L^{1-2})]$ and one mole of 4,4'-bipy was considered for the calculation of the DNA binding constant. The results indicate a comparable and nearly identical binding affinity for both the monomeric and dimeric complexes. This could be explained with the results of the stability studies in solution and DFT results which suggest that the 4,4'-bipy bridge of the dimeric complexes is broken in aqueous solution to give rise to two monomeric moieties. On the other hand, binding of CT DNA with the ligands alone do not reveal any significant interactions.

Competitive DNA binding fluorescence measurements

The exact mode of binding manifested by the complexes **1**–**4** with CT DNA was determined with three fluorescent dyes namely EB, DAPI and MG in 50 mM Tris–HCl buffer (pH 7.4) through competitive binding experiments, where EB

(ethidium bromide) binds to DNA through intercalation, DAPI (4′,6-diamidino-2-phenylindole) and MG (methyl green) are minor and major groove binders respectively.[17b,39] For the study, titration of an increasing complex concentration on EB bound to CT DNA, led to the quenching of the emission intensity of the latter adduct at 597 nm (**Figures S18-S19**). All the complexes exhibited a substantial displacement of the EB bound to CT DNA, which was in the range of ~50–75%. EB displacement parameters were also calculated through the same approach as described above for the binding interactions with HSA. Hence, the intercalative binding affinity of the complexes were evaluated using the Stern-Volmer equation, giving rise to K_{SV} values of 4.41 ± 0.32 × 10^3 M^{-1}, 4.35 ± 0.47 × 10^3 M^{-1}, 5.26 ± 0.35 × 10^3 M^{-1} and 4.95 ± 0.27 × 10^3 M^{-1} for complexes **1**–**4**, respectively. The relevant binding constants (K_b) are 1.85 ± 0.17 × 10^3 M^{-1}, 1.58 ± 0.37 × 10^3 M^{-1}, 7.33 ± 0.26 × 10^3 M^{-1} and 2.08 ± 0.20 × 10^3 M^{-1} for complexes **1**–**4**, respectively, and were derived from Scatchard equation. In this case too, the values are comparable, confirming the dissociation reactions in eqs. 1 and 2.

In addition, the minor groove binding affinity of **1**–**4** was assessed by the titration of DAPI bound CT DNA with increasing the complex concentration. There was a decrease in the emission intensity of the DAPI bound to CT DNA at 455 nm, indicating that the complexes could also interact with CT DNA through a minor groove binding (**Figures S20-S21)**. Quantitatively, complex **1**–**4** was found to be quenched of the emission intensity at 455 nm of ~70, ~66, ~85, ~75% respectively. Therefore, our results clearly demonstrate that the complexes **1**–**4** are able to interact with CT DNA through both intercalation and minor groove binding modes. We also performed similar competitive experiments with MG bound CT DNA; the results suggested that the Mo complexes were not able to quench the emission intensity at 597 nm (data not shown).

Circular Dichroism Study

Along with the above methods, circular dichroism (CD) spectroscopy was also used to study any conformational modifications taking place in CT DNA upon interaction with the metal complexes. As benchmark, the CD spectra of CT DNA alone reveal a positive band at 275 nm due to base stacking interaction and a negative band at 245 nm due to right handed helicity.[40] Generally, groove binding interactions shows little or no perturbation of the base stacking and helicity bands, while there is a change in the intensity of both bands for intercalation mode.[40b,41]

Owing to the interaction with the complexes **1**–**4**, the CD spectra of the CT DNA showed less change in the positive band at 275 nm, whereas a considerable change was observed in the negative band at 245 nm (**Figure 5**). The results suggested that, along with intercalative mode of binding which is quite evident from the spectra, the Mo complexes could also interact through groove binding and this is in good agreement with the competitive DNA binding results described above.

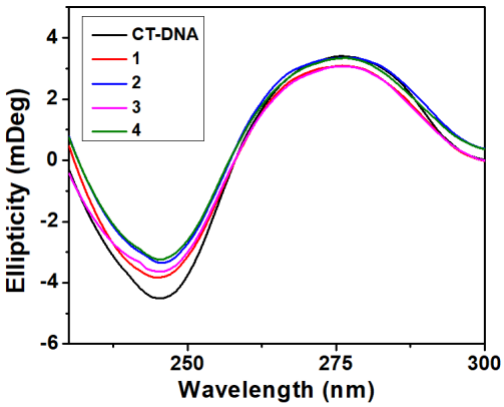

Figure 5 Circular dichroism spectra of CT DNA (100 μM) in the presence and absence of **1**–**4** in 50 mM Tris–HCl buffer (pH 7.4). The path length of the cuvette was 2 mm.

Cytotoxic activity and mechanism of action

Determination of the cytotoxic potential

In order to determine the cytotoxic effect of the Mo complexes, MTT cell viability assay was carried out.[15,17a,b,f] In the present investigation, the complexes – with a different number of metal centers and substituents in their ligand backbone – were tested for their toxicity on three different cell lines: human cervical cancer (HeLa), human colon cancer (HT-29) and noncancerous mouse embryonic fibroblast (NIH-3T3) cell lines.

Table 5 IC_{50} values of complexes **1**–**4** for HeLa, HT-29 and NIH-3T3 cell lines.

	IC_{50} (μM)		
Complex	**HeLa**	**HT-29**	**NIH-3T3**
1	10.29 ± 2.78	24.14 ± 0.96	41.47 ± 0.84
2	16.42 ± 3.94	25.68 ± 1.32	49.58 ± 0.37
3	9.73 ± 3.90	18.05 ± 1.53	48.60 ± 0.98
4	10.01 ± 2.22	25.04 ± 1.71	51.30 ± 0.52
Cisplatin	12.2	70	–

From the results, it can be established that the toxic effects are specific for each compound and are cell type dependent. The aroylhydrazone ligands does not show any significant toxicity compared to the complexes (IC_{50} > 100 μM), while the cytotoxicity of 4,4'-bipy is well established in the literature.[42] As compared to the other cancer cell line (HT-29), HeLa shows better sensitivity towards all the complexes, followed by HT-29 (**Figure 6**). The IC_{50} values indicate that these complexes may act differently on different cell lines ascertaining them to be cell specific. Overall, the IC_{50} values for Mo complexes (**Table 5**) were found comparable or also better than cisplatin, a commonly used chemo-therapeutic drug.[43]

The IC_{50} values for all the complexes have been calculated from the cell viability graph and are listed in **Table 5**. The results could be rationalized considering the behavior of **1**–**4** in aqueous solution. In particular, the dissociation of **3** and **4** complexes results in the release of two moles of penta-coordinated [MoO_2L^{1-2}] species and the cytotoxic 4,4'-bipy molecule. This mixture of species present in the incubation media may be responsible for comparatively

higher cytotoxicity of the dimeric complexes. This finding has been recently demonstrated where the active species could be more than one depending on the conditions; this is particularly evident for vanadium compounds, for which the ligand exchange, redox and chemical changes play a fundamental role to determine the active species in the organism.[7c,11,12,44] Therefore, similar type of behavior could be postulated for the present system. This insight further supports the data in the literature that for metal complexes, the biotransformation under biological media must be taken into account to explain the activity of a potential metal-based drug.

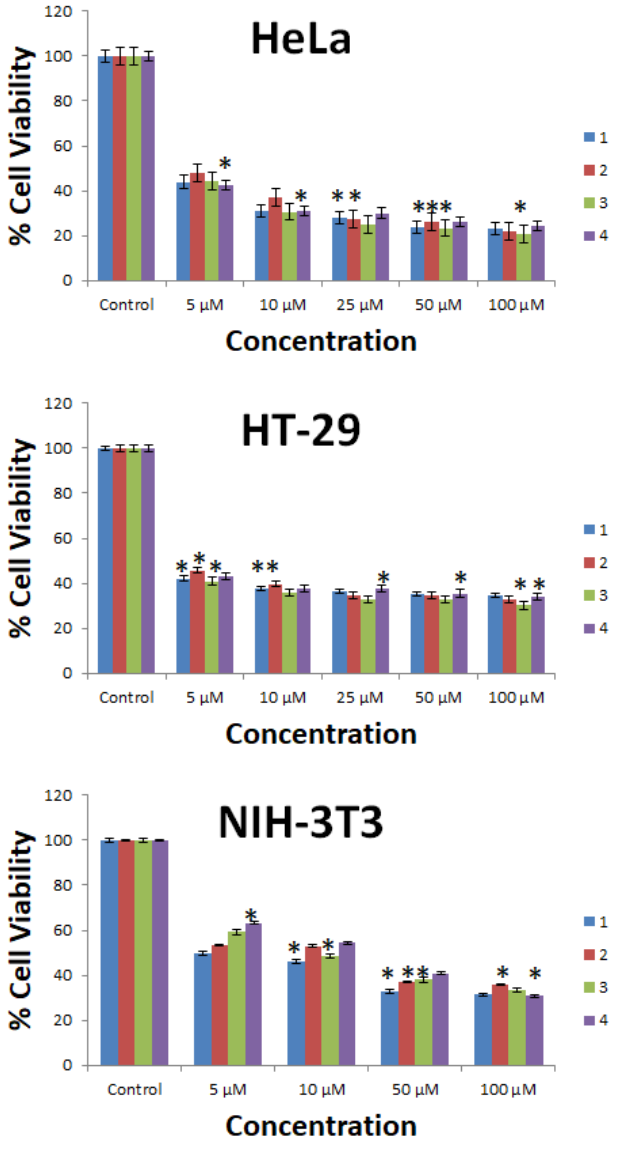

Figure 6 Cytotoxicity profiles of complexes **1**–**4** for HeLa, HT-29 and NIH-3T3 cell lines. The cells were subjected to treatment with varying concentrations of the Mo complexes for 48 h and the cell viability was measured using the MTT assay. Data are reported as the mean ± SD for n = 4 and * represents a statistical significance of $p<0.05$ as compared to the control.

So, as to establish the cell specificity of the complexes further and –in turn– study their anticancer properties, these complexes were evaluated for their cytotoxicity against noncancerous mouse embryonic fibroblast (NIH-3T3) cell line. The results demonstrated that they were significantly less toxic towards the noncancerous than cancerous cells (**Figure 6**). Therefore, it would be safe to claim that these complexes deserve to be further studied as potential anticancer agents in other cell lines in the future.

The present set of complexes has shown superior or similar cytotoxicity when compared to our investigations on other molybdenum(VI) complexes of aroylhydrazone ligands (IC_{50} between 4.41 and 162.55 µM for HeLa and IC_{50} between 20.63 and 177.92 µM for HT-29),[15,21d] salan (IC_{50} between 10.74 and 275.20 µM for HeLa and IC_{50} between 2.62 and 221.81 µM for HT-29).[17a] They are even better than what was reported for molybdenum(VI) complexes of Schiff base ligands (IC_{50} between 17 and 58 µM for HeLa[45]) and for molybdenum(V) complexes of neutral bidentate ligand (LC_{50} 35 µM for HeLa from other groups[46]).

Reduction by cellular reductants

Since complexes **1**–**4** contain Mo in the oxidation state +VI, their tendency to be reduced to a lower oxidation state has been verified by EPR, ESI-MS and UV-Vis spectroscopy, studying the reaction with cellular reducing agents such as L-ascorbic acid (Asc) and glutathione (GSH), which are present in the cellular environment.

The EPR studies were carried out in mixtures PBS/DMSO 1/1 (v/v) at physiological pH containing the reductants and the Mo complexes in molar ratios ranging from 1/1 to 10/1. In all the cases, the reduction of Mo^{VI} did not take place and it was not possible to reveal any spectral signals attributable to Mo^{V} which – having a $4d^1$ electronic configuration– is easily detectable by EPR.[47] However, a bielectronic reduction to Mo^{IV} ($4d^2$) could not be detectable by EPR due to the large zero-field splitting and fast relaxation time.[48] Therefore, by EPR the reduction to Mo^{V} but not to Mo^{IV} can be excluded.

To get other information on the possible reduction of **1** and **2**, several experiments were carried through the combined application of ESI-MS and UV-Vis with GSH and Asc in mixtures H_2O/MeOH, at different pH (5.0 and 7.4), metal concentration (5, 10 and 50 µM) and reductant/Mo ratio (1/1 and 10/1). In the ESI-MS spectra recorded with **1** only the peaks of $[MoO_2(L^1)]$ ($[MoO_2(L^1)]+H^+/Na^+/K^+$ at m/z 430.03, 452.01 and 467.99) and no signals of other Mo species were detected; moreover, the peaks of uncomplexed GSH ($[GSH]+H^+$ at m/z 308.09) and Asc ($[Asc]+H^+$ and $[Asc]+Na^+$ at m/z 199.02) are observed the possible peaks due to the oxidation products, GSSG and L-dehydroascobate (adducts with H^+ and Na^+ expected at m/z 613.16 and 635.15, and at 175.02 and 197.01, respectively) were not revealed (**Figure S22**). The UV-Vis spectra with $[MoO_2(L^{1-2})]$ do not show any appreciable variation, so the reduction and/or complexation could be excluded (**Figures 7 and S23**).

Therefore, the results demonstrate that the studied complexes are stable and do not have any tendency to be reduced even in the presence of cellular reductants. This finding has as a consequence that Fenton-like reactions, such as $Mo^{V}O^{3+} + H_2O_2 \rightarrow Mo^{VI}O_2^{2+} + H^+ + {}^{\bullet}OH$, are precluded for complexes **1**–**4** and that the mechanism of action could not be based on the production of ROS but on the direct interaction with DNA. This is only a hypothesis, but it seems to be rather plausible remembering that the

anticancerogenic activity of Mo^{VI} complexes has been explained with the binding to DNA or the production of reactive oxygen species (ROS); since it has been demonstrated that Mo^{VI} keeps its oxidation state, the formation of ROS should be precluded, so the cytotoxicity could be based on the interaction with DNA, which is possible as demonstrated in the section above.

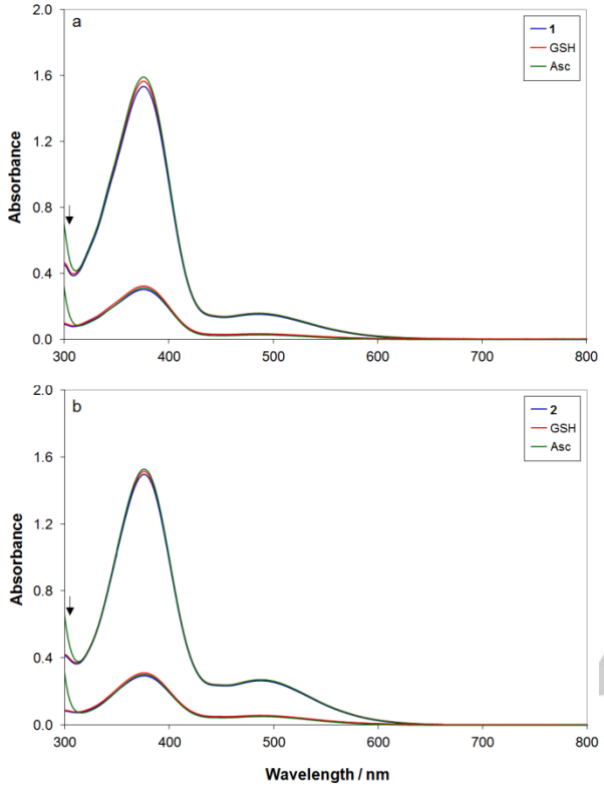

Figure 7 Electronic absorption spectra recorded on the systems containing [$MoO_2(L^{1-2})$] (**1**–**2**) and GSH or Asc with molar ratio 1/1, 50 and 10 μM, pH 7.4: a) **1**, H_2O/MeOH 90/10 v/v; b) **2**, H_2O/MeOH 80/20 v/v. With the arrow the absorption of Asc is shown.

Nuclear staining

The mode of cell death (apoptotic or necrotic) induced by the Mo complexes was determined through DAPI staining, which is a DNA binding dye. In line with MTT cell viability results, IC_{50} concentration of **1**–**4** was used in the staining study. Interestingly, it was observed that the complexes cause cell death through apoptotic pathway since the treated cells showed damaged DNA along with disrupted nuclear morphology, nuclear fragmentation and chromatin condensation. In contrast, the nucleus appeared perfectly intact in the control cells with a homogeneous shape (**Figure 8** and **S24**). This confirms that the mode of action of Mo compounds **1**–**4** must be explained with the interaction with DNA.

Conclusions

The results of the present study reveal that the transformation in biological media plays a key role in determining the active species and mode of action of the molybdenum compounds **1**–**4**. Both mononuclear **1** and **2** and dimeric **3** and **4** Mo complexes undergo chemical changes in solution to give the penta-coordinated species

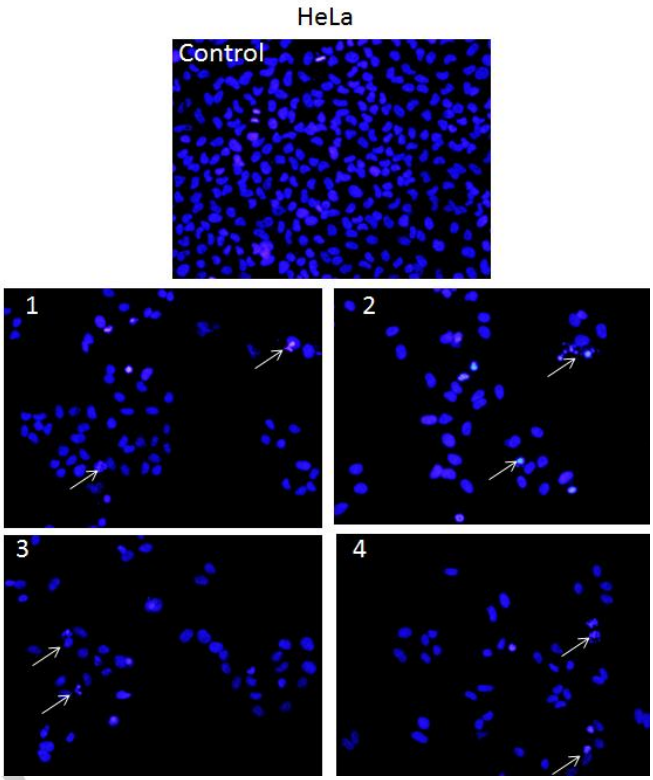

Figure 8 Changes of HeLa cells observed by fluorescence microscopy upon staining with DAPI following treatment with 1−4 (scale bar corresponds to 20 μm).

[MoO_2L^{1-2}]. This dissociation process should be taken into account in the analysis of the cytotoxicity of other polynuclear metal-based drugs. [MoO_2L^{1-2}] species are stable and, in the bloodstream, do not bind with low molecular mass bioligands. They only interact non-covalently with HSA before crossing the cellular membrane to enter in the cytosol. The results from the protein binding study suggested that the complexes could interact with HSA through static mode of quenching with reasonably good HSA binding parameters.

In the cytosol, Mo species are redox stable and keep the oxidation state of +VI even in the presence of strong reducing agents such as ascorbic acid or GSH. Since the reduction of Mo^{VI} to Mo^{V} or Mo^{IV} does not take place in the cellular environment, the mechanism of cellular toxicity of these complexes could not be related to the production of ROS through Fenton-like reaction; therefore, the cytotoxic activity shown by Mo species should be attributable to the direct binding with DNA. The complexes revealed moderately good DNA binding propensity through an intercalative and minor groove mode.

Further, the *in vitro* cytotoxicity of **1**−**4** was assayed against HeLa, HT-29 and NIH-3T3 cell lines. In spite being fairly cytotoxic in cancer cells, they were less toxic for the noncancerous cells. This could point towards a cancer cell specificity of the complexes. Moreover, among all the complexes, the mixed-ligand dimeric complexes (**3** and **4**) were comparatively better than their corresponding monomeric complexes (**1** and **2**) towards cytotoxicity. We hypothesize that this effect is due to the presence of mixture of [MoO_2L^{1-2}] species and 4,4'-bipy after the dissociation of dimeric **3** and **4** complexes.

The findings of this study should contribute towards the development of molybdenum-based anticancer agents and will pave a path to gain further insights into their mechanism of anticancer activity. Moreover, they confirm that often for a metal-based drug the transformation in biological media can be more important than the molecular nature of the synthesized species in the explanation of the pharmacological action. These chemical changes should be taken into account in the interpretation of the experimental results. In other words, the concept that the administered Mo complex may be only a prodrug, which releases the active species in the serum or cytosol, should be considered in the future in the rational design and development of new potential molybdenum drugs and their drug-delivery strategy.

Experimental and Computational Section

For all experimental details see the Supporting Information. CCDC reference numbers are 1997087 (complex **1**), 1997086 (complex **2**), 1997088 (complex **3**) and 1997089 (complex **4**).

Acknowledgements

R. D thanks DBT, Govt. of India [Grant No. 6242-P112/RGCB/ PMD/DBT/RPDA/2015] and CSIR, Govt. of India [Grant No. 01(2963)/18/EMR-II] for funding this research. R. D. also thanks Prof. Werner Kaminsky for help in crystallographic section. G.S., D.S., V.U., and E.G. are thankful to Regione Autonoma della Sardegna (grant RASSR79857) and Fondazione di Sardegna (grant 2017) for financial support.

Conflict of interest

The authors declare no conflict of interest.

Keywords: Mo(VI) • Aroylhydrazones • Metallodrugs • Protein and DNA interaction • Cytotoxicity

References

[1] a) N. J. Wheate, S. Walker, G. E. Craig, R. Oun, *Dalton Trans.* **2010**, *39*, 8113–8127; b) A. Levina, A. Mitra, P. A. Lay, *Metallomics : integrated biometal science* **2009**, *1*, 458–470.

[2] J. Flarakos, K. L. Morand, P. Vouros, *Anal. Chem.* **2005**, *77*, 1345–1353.

[3] a) W. O. Foye, Cancer Chemotherapeutic Agents, American Chemical Society, Washington, DC, 1995, ISBN 0-8412-2920-1; b) F. Arnesano, M. Losacco, G. Natile, *Eur. J. Inorg. Chem.* **2013**, *2013*, 2701−2711; c) J. D. Hoeschele, *Dalton Trans.* **2009**, 10648−10650; d) J. Reedijk, *Eur. J. Inorg. Chem.* **2009**, *2009*, 1303−1312; e) M. Raudenska, J. Balvan, M. Fojtu, J. Gumulec, M. Masarik, *Metallomics* **2019**, *11*, 1182-1199.

[4] a) O. Kennard, *Pure Appl. Chem.* **1993**, *65*, 1213–1222; b) R. Hajian, N. Shams, M. Mohagheghian, *J. Braz. Chem. Soc.* **2009**, *20*, 1399–1405.

[5] a) C. J. Jones, J. R. Thornback, *Medicinal applications of coordination chemistry;* Royal Society of Chemistry, **2007**; b) J. C. Dabrowiak, *Metals in Medicine;* John Wiley & Sons Ltd, Chichester, U.K, **2009**.

[6] a) M. Guo, P. J. Sadler, *J. Chem. Soc., Dalton Trans.* **2000**, 7–9; b) O. Ulrike, H. Gerhard, *Anti-Cancer Agents Med. Chem.* **2010**, *10*, 302–311.

[7] a) S. Spreckelmeyer, C. Orvig, A. Casini, *Molecules* **2014**, *19*, 15584-15610; b) A. Merlino, T. Marzo, L. Messori, *Chem. Eur. J.* **2017**, *23*, 6942-6947; c) A. Levina, D. C. Crans, P. A. Lay, *Coord. Chem. Rev*. **2017**, *352*, 473-498; d) C. I. Yeo, K. K. Ooi, E. R. T. Tiekink, *Molecules* **2018**, *23*, 1410; e) Metallo-Drugs: Development and Action of Anticancer Agents, De Gruyter, **2018**; f) T. Kiss, É. A. Enyedy, T. Jakusch, O. Dömötör, *Curr. Med. Chem*. **2019**, *26*, 580-606; g) E. J. Anthony, E. M. Bolitho, H. E. Bridgewater, O. W. L. Carter, J. M. Donnelly, C. Imberti, E. C. Lant, F. Lermyte, R. J. Needham, M. Palau, P. J. Sadler, H. Shi, F.-X. Wang, W.-Y. Zhang, Z. Zhang, *Chem. Sci*. **2020**, *11*, 12888-12917; h) A. Merlino, *Chem. Commun*. **2021**, *57*, 1295-1307.

[8] a) C. Billecke, S. Finniss, L. Tahash, C. Miller, T. Mikkelsen, N. P. Farrell, O. Bögler, *Neuro-Oncol*. **2016**, *8*, 215-226; b) M. P. M. Marques, ISRN Spectroscopy **2013**, *2013*, 287353; c) T.S. Reddy, D. Pooja, S. H. Privér, R. B. Luwor, N. Mirzadeh, S. Ramesan, S. Ramakrishna, S. Karri, M. Kuncha, S. K. Bhargava, *Chem. Eur. J.* **2019**, *25*, 14089-14100; d) S. Radisavljević, B. Petrović, *Front. Chem.* **2020**, *8*, 379.

[9] a) S. B. Etcheverry, A. L. Di Virgilio, O. R. Nascimento, P. A. M. Williams, *J. Inorg. Biochem*. **2012**, *107*, 25-33; b) T. A. Fernandes, F. Mendes, A. P. S. Roseiro, I. Santos, M. F. N. N. Carvalho, *Polyhedron* **2015**, *87*, 215-219; c) M. Cindrić, A. Bjelopetrović, G. Pavlović, V. Damjanović, J. Lovrić, D. Matković-Čalogović, V. Vrdoljak, *New J. Chem*. **2017**, *41*, 2425-2435; d) A. Bhunia, S. Mistri, R. K. Manne, M. K. Santra, S. C. Manna, *Inorg. Chim. Acta* **2019**, *491*, 25-33.

[10] a) J. C. Jeffery, J. P. Maher, C. A. Otter, P. Thornton, M. D. Ward, *J. Chem. Soc., Dalton Trans*. **1995**, 819-824; b) G. van Albada, I. Mutikainen, W. J. J. Smeets, A. L. Spek, U. Turpeinen, J. Reedijk, *Inorg. Chim. Acta* **2002**, *327*, 134-139; c) W. A. Alves, R. H. de Almeida Santos, A. Paduan-Filho, C. C. Becerra, A. C. Borin, A. M. Da Costa Ferriera, *Inorg. Chim. Acta* **2004**, *357*, 2269-2278; d) M. A. Ali, A. H. Mirza, R. J. Fereday, R. J. Butcher, J. M. Fuller, S. C. Drew, L. R. Gahan, G. R. Hanson, B. Moubaraki, K. S. Murray, *Inorg. Chim. Acta* **2005**, *358*, 3937-3948; e) I. A. Koval, M. Sgobba, M. Huisman, M. Lüken, E. Saint-Aman, P. Gamez, B. Krebs, J. Reedijk, *Inorg. Chim. Acta* **2006**, *359*, 4071-4078; f) S. Thakurta, J. Chakraborty, G. Rosair, J. Tercero, M.S. El Fallah, E. Garribba, S. Mitra, *Inorg. Chem*. **2008**, *47*, 6227-6235; g) S. Thakurta, P. Roy, G. Rosair, C.J. Gómez-García, E. Garribba, S. Mitra, *Polyhedron* **2009**, *28*, 695-702; h) A. Ray, C. Rizzoli, G. Pilet, C. Desplanches, E. Garribba, E. Rentschler, S. Mitra, *Eur. J. Inorg. Chem*. **2009**, 2915-2928; i) C. P. Pradeep, S. K. Das, *Polyhedron* **2009**, *28*, 630-636; j) S. Thakurta, C. Rizzoli, R. J. Butcher, C. J. Gómez-García, E. Garribba, S. Mitra, *Inorg. Chim. Acta* **2010**, *363*, 1395-1403; k) S. Shit, M. Nandy, G. Rosair, M. Salah El Fallah, J. Ribas, E. Garribba, S. Mitra, *Polyhedron* **2013**, *52*, 963-969; l) S. Saha, A. Sasmal, C. R. Choudhury, C. J. Gomez-Garcia, E. Garribba, S. Mitra, *Polyhedron* **2014**, *69*, 262-269.

[11] A. Banerjee, S. P. Dash, M. Mohanty, G. Sahu, G. Sciortino, E. Garribba, Carvalho, M. Fernanda N. N, F. Marques, J. Costa Pessoa, W. Kaminsky, K. Brzezinski, R. Dinda, *Inorg. Chem.* **2020**, *59*, 14042–14057.

[12] Y. Yoshikawa, H. Sakurai, D. C. Crans, G. Micera, E. Garribba, *Dalton Trans.* **2014**, *43*, 6965–6972.

[13] V. Vrdoljak, I. Đilović, M. Rubčić, S. K. Pavelić, M. Kralj, D. Matković–Čalogović, I. Piantanida, P. Novak, A. Rožman, M. Cindrić, *Eur. J. Med. Chem.* **2010**, *45*, 38–48.

[14] a) A. Jurowska, K. Jurowski, J. Szklarzewicz, B. Buszewski, T. Kalenik, W. Piekoszewski, *Curr. Med. Chem.* **2016**, *23*, 3322–3342; b) A. T. Odularu, P. A. Ajibade, J. Z. Mbese, *Bioinorg. Chem. Appl.* **2019**, *2019*; c) S. Majumder, S. Pasayat, A. K. Panda, S. P. Dash, S. Roy, A. Biswas, M. E. Varma, B. N. Joshi, E. Garribba, C. Kausar, *Inorg. Chem.* **2017**, *56*, 11190–11210; d) J. M. Gretarsdóttir, S. Bobersky, N. Metzler-Nolte, S. G. Suman, *J. Inorg. Biochem.* **2016**, *160*, 166–171; e) P. M. Abeysinghe, M. M. Harding, *Dalton Trans.* **2007**, 3474–3482; f) S. Gomez-Ruiz, D. Maksimović-Ivanić, S. Mijatović, G. N. Kaluđerović, *Bioinorg. Chem. Appl.* **2012**, *2012*; g) J. Honzíček, J. Vinklárek, M. Erben, Z. Padělková, L. Šebestová, M. Řezáčová, *J. Organomet. Chem.* **2014**, *749*, 387–393; h) Matos, M. R. P. N. d, C. C. Romão, C. C. L. Pereira, S. S. Rodrigues, M. Mora, M. J. P. Silva, P. M. Alves, Reis, C. A. International Patent WO/2005/08778.

[15] R. Dinda, A. Panda, A. Banerjee, M. Mohanty, S. Pasayat, E. R. T. Tiekink, *Polyhedron* **2020**, *183*, 114533–114545.

[16] M. L. Nair, D. Thankaman, *Indian J. Chem*. **2009**, *48A*, 1212–1218.

[17] a) S. Roy, M. Mohanty, S. Pasayat, S. Majumder, K. Senthilguru, I. Banerjee, M. Reichelt, H. Reuter, E. Sinn, R. Dinda, *J. Inorg. Biochem.* **2017**, *172*, 110–121; b) A. Chakraborty, S. P. Dash, A. K. Panda, R. Acharyya, A. Biswas, S. Mukhopadhyay, S. K. Bhutia, A. Crochet, Y. P. Patil, M. Nethaji, *Dalton Trans.* **2015**, *44*, 6140–6157; c) S. Roy, M. Böhme, S. P. Dash, M. Mohanty, A. Buchholz, W. Plass, S. Majumder, S. Kulanthaivel, I. Banerjee, H. Reuter, *Inorg. Chem.* **2018**, *57*, 5767–5781; d) S. Pasayat, S. P. Dash, S. Roy, R. Dinda, S. Dhaka, M. R. Maurya, W. Kaminsky, Y. P. Patil, M. Nethaji, *Polyhedron* **2014**, *67*, 1–10; e) M. Mohanty, A. Banerjee, S. Biswal, A. Horn Jr, G. Schenk, K. Brzezinski, E. Sinn, H. Reuter, R. Dinda, *J. Inorg. Biochem.* **2020**, *203*, 110908; f) S. Roy, M. Mohanty, R. G. Miller, S. A. Patra, S. Lima, A. Banerjee, N. Metzler-Nolte, E. Sinn, W. Kaminsky, R. Dinda, *Inorg. Chem.* **2020**, *59*, 15526–15540.

[18] a) B. K. Kaymakçıoğlu, S. Rollas, *Il Farmaco* **2002**, *57*, 595–599; b) Ş. G. Küçükgüzel, S. Rollas, I. Küçükgüzel, M. Kiraz, *Eur. J. Med. Chem.* **1999**, *34*, 1093–1100; c) S. Zhang, A. D. Sherry, *J. Solid State Chem.* **2003**, *171*, 38–43; d) Z.-Y. Yang, *Synth. React. Inorg. Met.-Org. Chem.* **2000**, *30*, 1265–1271.

[19] P. Krishnamoorthy, P. Sathyadevi, A. H. Cowley, R. R. Butorac, N. Dharmaraj, *Eur. J. Med. Chem.* **2011**, *46*, 3376–3387.

[20] a) D. Wesselinova, M. Neykov, N. Kaloyanov, R. Toshkova, G. Dimitrov, *Eur. J. Med. Chem.* **2009**, *44*, 2720–2723; b) S. Jagadeesan, V. Balasubramanian, P. Baumann, M. Neuburger, D. Häussinger, C. G. Palivan, *Inorg. Chem.* **2013**, *52*, 12535–12544.

[21] a) J. H. Enemark, J. J. A. Cooney, J.-J. Wang, R. H. Holm, *Chem. Rev.* **2004**, *104*, 1175–1200; b) R. Dinda, P. Sengupta, S. Ghosh, W. S. Sheldrick, *Eur. J. Inorg. Chem.* **2003**, *2003*, 363–369; c) R. Dinda, S. Ghosh, L. R. Falvello, M. Tomás, T. C. W. Mak, *Polyhedron* **2006**, *25*, 2375–2382; d) S. Pasayat, S. P. Dash, S. Majumder, R. Dinda, E. Sinn, H. Stoeckli-Evans, S. Mukhopadhyay, S. K. Bhutia, P. Mitra, *Polyhedron* **2014**, *80*, 198–205; e) S. Purohit, A. P. Koley, L. S. Prasad, P. T. Manoharan, S. Ghosh, *Inorg. Chem.* **1989**, *28*, 3735–3742.

[22] R. Dinda, P. Sengupta, S. Ghosh, H. Mayer-Figge, W. S. Sheldrick, *Dalton Trans.* **2002**, 4434–4439.

[23] A. V. Marenich, C. J. Cramer, D. G. Truhlar, *J. Phys. Chem. B* **2009**, *113*, 6378–6396.

[24] (a) S. Al-Harthi, J. I. Lachowicz, M. E. Nowakowski, M. Jaremko, Ł. Jaremko, *J. Inorg. Biochem.* **2019**, *198*, 110716; (b) G. Sciortino, D. Sanna, G. Lubinu, J.-D. Maréchal, E. Garribba, *Chem.–Eur. J.* **2020**, *26*, 11316-11326.

[25] S. Lin, S. T. Wrobleski, J. Hynes, S. Pitt, R. Zhang, Y. Fan, A. M. Doweyko, K. F. Kish, J. S. Sack, M. F. Malley, S. E. Kiefer, J. A. Newitt, M. McKinnon, J. Trzaskos, J. C. Barrish, J. H. Dodd, G. L. Schieven, K. Leftheris, *Bioorg. Med. Chem. Lett.* **2010**, *20*, 5864–5868.

[26] M. Dąbrowska, M. Starek, J. Skuciński, *Talanta* **2011**, *86*, 35–51.

[27] a) C. K. Mirabelli, R. K. Johnson, C. M. Sung, L. Faucette, K. Muirhead, S. T. Crooke, *Canc. Res.* **1985**, *45*, 32–39; b) V. T. Yilmaz, C. Icsel, O. R. Turgut, M. Aygun, M. Erkisa, M. H. Turkdemir, E. Ulukaya, *Eur. J. Med. Chem.* **2018**, *155*, 609–622.

[28] a) J. Wang, Y. Gou, Z. Zhang, P. Yu, J. Qi, Q. Qin, H. Sun, X. Wu, H. Liang, F. Yang, *Mol. Pharm.* **2018**, *15*, 2180–2193; b) Y. Gou, J. Qi, J.-P. Ajayi, Y. Zhang, Z. Zhou, X. Wu, F. Yang, H. Liang, *Mol. Pharm.* **2015**, *12*, 3597–3609.

[29] a) A. Hussain, M. F. AlAjmi, M. T. Rehman, S. Amir, F. M. Husain, A. Alsalme, M. A. Siddiqui, A. A. AlKhedhairy, R. A. Khan, *Scientific reports* **2019**, *9*, 1–17; b) I. L. Medintz, N. Hildebrandt, *FRET-Förster resonance energy transfer: from theory to applications;* John Wiley & Sons, **2013**.

[30] S. U. Parsekar, P. Velankanni, S. Sridhar, P. Haldar, N. A. Mate, A. Banerjee, P. S. Antharjanam, A. P. Koley, M. Kumar, *Dalton Trans.* **2020**, *49*, 2947–2965.

[31] a) M. T. Rehman, H. Shamsi, A. U. Khan, *Mol. Pharm.* **2014**, *11*, 1785–1797; b) Z. Xu, Y. Liu, S. Zhou, Y. Fu, C. Li, *Int. J. Mol. Sci.* **2016**, *17*, 1042.

[32] a) M. S. Ali, M. Amina, H. A. Al-Lohedan, N. M. Al Musayeib, *Luminescence* **2017**, *32*, 223–230; b) Y. Yue, Y. Sun, Q. Dong, R. Liu, X. Yan, Y. Zhang, J. Liu, *Luminescence* **2016**, *31*, 671–681.

[33] D. Sanna, G. Delogu, M. Mulas, M. Schirra, A. Fadda, *Food Anal. Methods* **2012**, *5*, 759–766.

[34] R. Re, N. Pellegrini, A. Proteggente, A. Pannala, M. Yang, C. Rice-Evans, *Free Rad. Biol. Med.* **1999**, *26*, 1231–1237.

[35] A. Fadda, D. Sanna, *Advances in Food Analysis Research; Nova Science Publisher, Inc.: Hauppauge, NY, USA* **2015**, 65–88.

[36] a) C. X. Zhang, S. J. Lippard, *Curr. Opin. Chem. Biol.* **2003**, *7*, 481–489; b) L. R. Ferguson, W. A. Denny, *Mutat. Res./Fundam. Mol. Mech. Mutagen.* **2007**, *623*, 14–23; c) K. Gkionis, J. A. Platts, J. G. Hill, *Inorg. Chem.* **2008**, *47*, 3893–3902; d) Janice R. Aldrich-Wright, Robert S. Vagg, Peter A. Williams, *Coord. Chem. Rev.* **1997**, *166*, 361–389; d) Y. Jung, S. J. Lippard, *Chem. Rev.* **2007**, *107*, 1387–1407.

[37] a) T. S. Kamatchi, N. Chitrapriya, S. K. Kim, F. R. Fronczek, K. Natarajan, *Eur. J. Med. Chem.* **2013**, *59*, 253–264; b) S. E. Sherman, D. Gibson, A. H. J. Wang, S. J. Lippard, *J. Am. Chem. Soc.* **1988**, *110*, 7368–7381; c) L. Strekowski, B. Wilson, *Mutat. Res.* **2007**, *623*, 3–13.

[38] M. Ganeshpandian, R. Loganathan, E. Suresh, A. Riyasdeen, M. A. Akbarsha, M. Palaniandavar, *Dalton Trans.* **2014**, *43*, 1203–1219.

[39] a) S. Satpathi, A. Sengupta, V. M. Hridya, K. Gavvala, R. K. Koninti, B. Roy, P. Hazra, *Sci. Rep.* **2015**, *5*, 9137; b) D. Prieto, G. Aparicio, P. E. Morande, F. R. Zolessi, *Histochem. Cell Biol.* **2014**, *142*, 335–345.

[40] a) L. Tjioe, A. Meininger, T. Joshi, L. Spiccia, B. Graham, *Inorg. Chem.* **2011**, *50*, 4327–4339; b) K. Karidi, A. Garou, *Dalton Trans.* **2005**, *1176*.

[41] V. Ivanov, Le Minchenkova, A. K. Schyolkina, A. I. Poletayev, *Biopolymers: Original Research on Biomolecules* **1973**, *12*, 89–110.

[42] a) M. Michel-Buono, J.-P. Buono, G. Serre, D. Dumont, P. Bernard, *Cell Biol. Toxicol.* **1997**, *13*, 193–204; b) S. Li, P. A. Crooks, X. Wei, J. Leon, *Crit. Rev. Toxicol.* **2004**, *34*, 447–460.

[43] a) L. Reytman, O. Braitbard, E. Y. Tshuva, *Dalton Trans.* **2012**, *41*, 5241–5247; b) A. Stockert, D. Kinder, M. Christ, K. Amend, A. Aulthouse, *Austin J Pharmacol Ther.* **2014**, *2*, 6.

[44] a) M. Le, O. Rathje, A. Levina, P. A. Lay, *JBIC, J. Biol. Inorg. Chem,* **2017**, *22*, 663–672; b) E. Griffin, A. Levina, P. A. Lay, *J. Inorg. Biochem.* **2019**, *201*, 110815; c) D. Sanna, J. Palomba, G.

Lubinu, P. Buglyó, S. Nagy, F. Perdih, E. Garribba, *J. Med. Chem.* **2019**, *62*, 654–664; d) P. Nunes, I. Correia, I. Cavaco, F. Marques, T. Pinheiro, F. Avecilla, J. Costa Pessoa, *J. Inorg. Biochem.* **2021**, *217*, 111350; e) J. Costa Pessoa, I. Correia, *Inorganics,* **2021**, *9*, 17.

[45] Z. Kazemi, H. A. Rudbari, M. Sahihi, V. Mirkhani, M. Moghadam, S. Tangestaninejad, I. Mohammadpoor-Baltork, A. A. Kajani, *Polyhedron* **2019**, *170*, 70–85.

[46] M. Roy, D. Biswal, O. Sarkar, N. R. Pramanik, M. G. B. Drew, P. Sadhukhan, M. Kundu, P. C. Sil, S. Chakrabarti, *J. Inorg. Biochem.* **2019**, *199*, 110755.

[47] a) A. Rajapakshe, R. A. Snyder, A. V. Astashkin, P. Bernardson, D. J. Evans, C. G. Young, D. H. Evans, J. H. Enemark, *Inorg. Chim. Acta* **2009**, *362*, 4603–4608; b) C. Prior, L. R. Webster, S. K. Ibrahim, J. A. Wright, A. F. Alghamdi, V. S. Oganesyan, C. J. Pickett, *Dalton Trans.* **2016**, *45*, 2399–2403; c) G. Hanson, L. Berliner, *Metals in biology: Applications of high-resolution EPR to metalloenzymes;* Springer, **2010**.

[48] a) R. S. Drago, Physical Methods in Chemistry W, B. Saunders Company, Philadelphia, **1977**; b) F. E. Mabbs, D. Collison, Electron Paramagnetic Resonance of d Transition Metal Compounds, Elsevier Science Publishers B.V., Amsterdam, **1992**.

WILEY-VCH

Entry for the Table of Contents

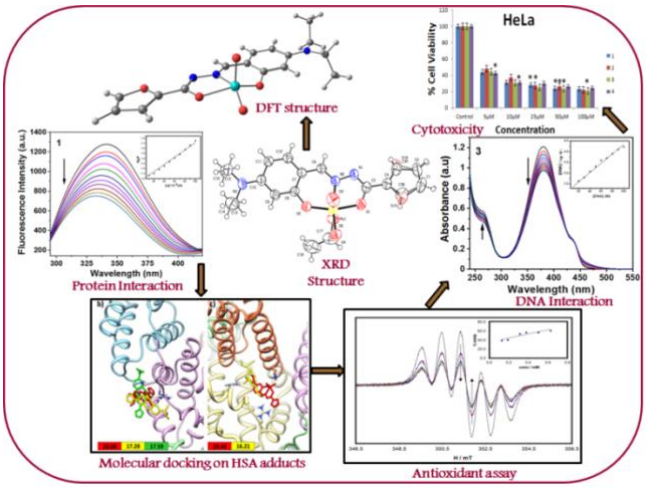

The transformation of a series of mono and dimeric molybdenum(VI) complexes in biological media, their interaction with biomolecules and *in vitro* cytotoxicity has been studied. Both the species undergo chemical changes in solution to give the penta-coordinated species [$MoO_2(L^{1-2})$]. The enhanced biological potential revealed by the dimeric complexes have been attributed to the mixture of [$MoO_2(L^{1-2})$] species and the cytotoxic 4,4'-bipy molecule.